Reaction Mechanism of [NiFe] Hydrogenase Studied by Computational Methods

Dong, Geng; Phung, Quan Manh; Pierloot, Kristine; Ryde, Ulf

Published in:
Inorganic Chemistry

DOI:
10.1021/acs.inorgchem.8b02590

2018

Document Version:
Peer reviewed version (aka post-print)

Reaction mechanism of [NiFe] hydrogenase studied by computational methods

Geng Dong,[a,b] Quan Manh Phung,[c] Kristine Pierloot,[c] Ulf Ryde [a]*

[a] Department of Theoretical Chemistry, Lund University, Chemical Centre, P. O. Box 124, SE-221 00 Lund, Sweden

[b] Department of Biochemistry and Molecular Biology, Shantou University Medical College, Shantou 514041, Guangdong, PR China

[c] Department of Chemistry, KU Leuven, Celestijnenlaan 200F, B-3001 Leuven, Belgium

Correspondence to Ulf Ryde, email: Ulf.Ryde@teokem.lu.se

2018-10-30

Abstract
[NiFe] hydrogenases catalyse the reversible conversion of molecular hydrogen to protons and electrons. This seemingly simple reaction has attracted much attention because of the prospective use of H_2 as a clean fuel. In this paper, we have studied the full reaction mechanism of this enzyme with various computational methods. Geometries were obtained with combined quantum mechanical and molecular mechanics (QM/MM) calculations. To get more accurate energies and obtain a detailed account of the surroundings, we performed big-QM calculations with 819 atoms in the QM region. Moreover, QM/MM thermodynamic-cycle perturbations (QTCP) calculations were performed to obtain free energies. Finally, density matrix renormalisation group complete active space self-consistent field (DMRG-CASSCF) calculations were carried out to study the electronic structures of the various states in the reaction mechanism. Our calculations indicate that the Ni-L state is not involved in the reaction mechanism. Instead the Ni-C state is reduced by one electron and then the bridging hydride ion is transferred to the sulfur atom of Cys546 as a proton and the two electrons transfer to Ni ion. This step turned out to be rate-determining with an energy barrier of 58 kJ/mol, which is consistent with the experimental rate of 750±90 s^{-1} (corresponding to ~52 kJ/mol). The cleavage of H–H bond is facile with an energy barrier of 33 kJ/mol according to our calculations. We also find that the reaction energies are sensitive to the size of QM system, the basis set and the density-functional theory method, in agreement with previous studies.

Keywords: [NiFe] hydrogenase, reaction mechanism, density-functional theory, DMRG-CASSCF, QM/MM, big-QM, QTCP.

Introduction

Hydrogenases are metalloenzymes that catalyse the reversible conversion of protons and electrons to H_2. As H_2 has a promising potential as a non-carbon energy carrier, hydrogenases have attracted much interest and have been studied extensively.[1-3] The hydrogenases can be classified into three groups based on the metal content of the active site, viz. [Fe], [FeFe] and [NiFe] hydrogenases.

Numerous crystallographic studies have presented structures of hydrogenases.[4] For [NiFe] hydrogenases, the active site contains one Ni and one Fe ion. The iron ion is coordinated by one carbon monoxide and two cyanide molecules. In addition, two thiolates from Cys84 and 549 (residues are numbered according to the enzyme from *Desulfovibrio vulgaris* Miyazaki F[5]) bridge the two metals. The nickel ion has two additional cysteine ligands (Cys81 and 546) that are terminally coordinated. Typically, the [NiFe] hydrogenases also contain three FeS clusters and an octahedral Mg^{2+} site.

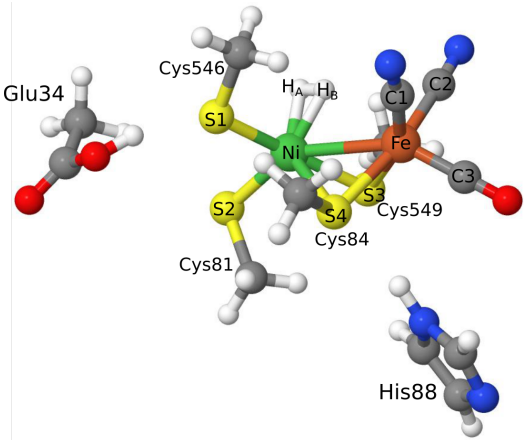

Figure 1. The active site of the [NiFe] hydrogenases with H_2 binding to the Ni ion (QM/MM structure of the Ni-H2 state).

Three spectroscopic states have been found to participate in the catalytic cycle of the [NiFe] hydrogenases, viz. the Ni-SI_a, Ni-C and Ni-R states.[1] The Ni-SI_a state is EPR-silent[6] and it is widely accepted that both metals are in the +II oxidation state (in fact, the iron ion remains in the low-spin +II state throughout the reaction cycle[7, 8]). Moreover, it probably does not contain any extra ligands in the active site, i.e. the iron ion is penta-coordinate and the nickel ion is tetra-coordinate. The Ni-SI_a state is ready to react with the hydrogen molecule. The Ni-C state is generated during the activation of H_2 and it is paramagnetic with a Ni(III) ion.[9] In this state, a hydrogen species (a hydride ion) probably bridges the two metals.[9] One-electron reduction of the Ni-C state leads to the Ni-R state. The Ni-R state is also EPR-silent with the same oxidation state of the two metal ions as in the Ni-SI_a state, i.e. Fe(II) and Ni(II). A recent high-resolution (0.89 Å) X-ray structure of Ni-R shows that a hydride ion is bridging the Ni and Fe ions and the terminal Cys546 residue is protonated.[10]

Moreover, an additional state, called Ni-L, can be generated from Ni-C by illumination.[11-15] In this paramagnetic state, the bridging hydride ligand has dissociated, most likely as a proton.[14] However, the oxidation state of the Ni ion is unclear. On the one hand, it has been suggested to be +I by EPR experiments[12, 14-16] and this is also the expected state if a proton dissociates from a Ni(III)–hydride complex. On the other hand, X-ray absorption studies indicate that it is closer to Ni(III) than to Ni(I).[17] Recently, the Ni-L state was found also in dark environment, indicating that the Ni-L state may be involved in the catalytic cycle.[18, 19]

In our previous studies, we have studied the protonation states of the cysteine residues in the active site of [NiFe] hydrogenase for the Ni-SI$_a$, Ni-R, Ni-C and Ni-L states, as well as H_2 binding to Ni-SI$_a$.[20-22] These studies showed that Cys546 is the most easily protonated residue for all states during the reaction and that H_2 binds to the Ni ion in the singlet state. However, the full reaction mechanism is still unclear.

Early theoretical studies of the reaction mechanism of [NiFe] hydrogenases proposed that H_2 binds to Fe ion and is cleaved heterolytically.[23, 24] Hall and coworkers suggested that that cleavage of H_2 is more favourable if the nickel ion is oxidised to Ni(III) than with Ni(II) (shown with orange arrows in Figure 2)[23] and later that Ni is in the high-spin state.[25] On the other hand, in 2009, Siegbahn and coworkers suggested an oxidative addition mechanism (shown with yellow arrows in Figure 2), in which H_2 binds to Ni ion of Ni-L and is cleaved in the Ni(I) state, because the heterolytic cleavage of the H–H bond by Ni(II) gave a rather high energy barrier, 67 kJ/mol, whereas it was 49 kJ/mol with Ni(I).[26] Thus, they suggest that the H_2 binding to Ni-SI$_a$ is just as an initial step to generate the Ni-L state, whereas the actual reaction cycle involves Ni-R, Ni-C and Ni-L, but not Ni-SI$_a$.

Moreover, in two recent theoretical studies, three different reaction mechanisms were suggested, as shown in Figure 2.[27, 28] In the mechanism suggested by Sun and coworkers (shown with black arrows in Figure 2), H_2 binds to Ni-SI$_a$, forming a Ni-H2 state, which is still in the Ni(II) oxidation state.[27] Then, the H–H bond is cleaved, forming the Ni-R state directly with one proton on Cys546 and a bridging hydride ion: The activation energy was 38 kJ/mol and the reaction was exothermic by 15 kJ/mol. Next, the proton dissociates to the solvent and the active site is oxidised, giving rise to the Ni-C state. In the following step, Ni-C is converted to Ni-L by the movement of the bridging hydride ion to Cys546, i.e. by converting the hydride ion to a proton and reducing the Ni ion from +III to +I. They obtained an energy barrier of 64 kJ/mol for this step and the reaction was endothermic by 29 kJ/mol.[27] Finally, the proton dissociates again to the solvent and the site is oxidised to form the starting Ni-SI$_a$ state.

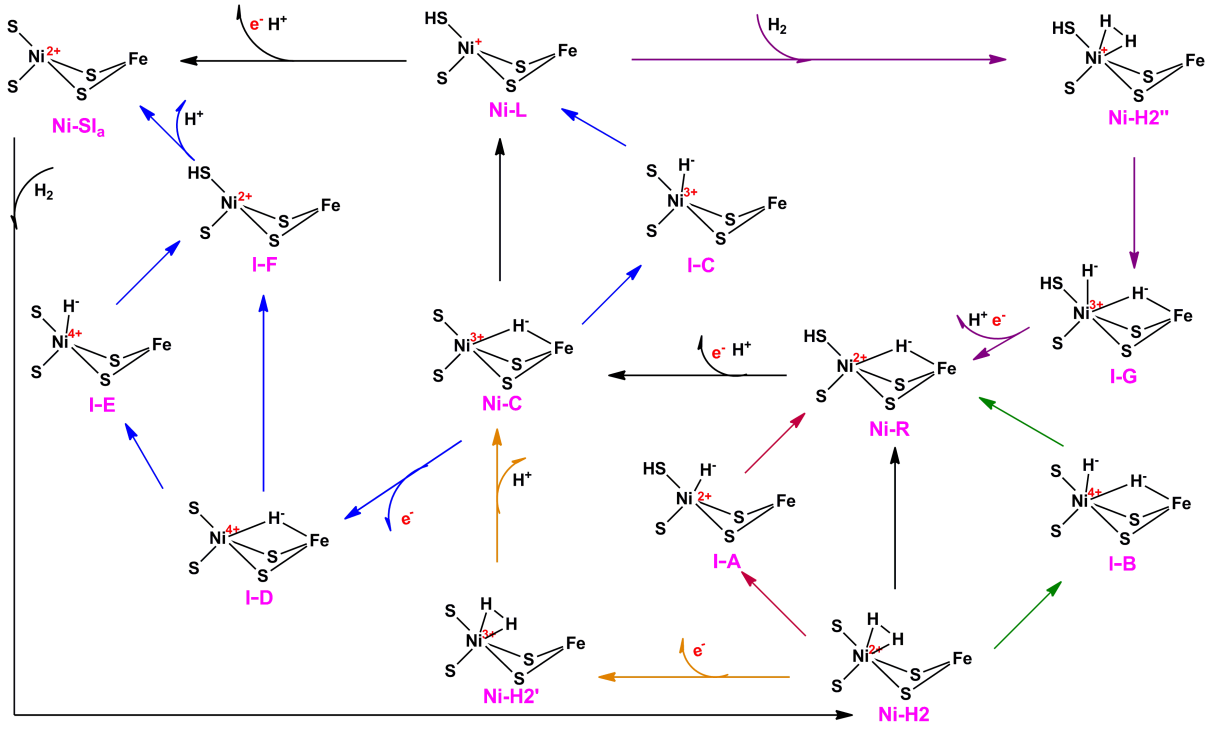

Figure 2. Reaction mechanisms suggested by theoretical studies. All the hydrogen species binding to Ni are supposed to be hydride ions.

Bruschi and coworkers studied the reaction mechanism for the H_2 cleavage from the Ni-H2 state to the Ni-R state.[28] They could not obtain any direct conversion between these two states, but instead studied two mechanisms with one intermediate each, viz. Ni-H2→I-A (intermediate state A)→Ni-R and Ni-H2→I-B→Ni-R, as shown with red and green arrows in Figure 2. In the former mechanism, the calculated energy barriers of the two steps were 52 and 13 kJ/mol, respectively, and the two reactions were endothermic by 5 kJ/mol and exothermic by 26 kJ/mol, respectively. In the other mechanism, involving the I-B state, the activation energies were lower, viz. both 5 kJ/mol. The reactions of the two steps in the latter mechanism were both exothermic, by 0.4 and 21 kJ/mol, respectively. Thus, the reaction mechanism involving I-B was found to be more favourable than that involving I-A. However, they did not study the remaining part of the reaction mechanism.

Thus, the suggested reaction mechanisms obtained by QM-cluster methods differ in several aspects: a) Is the Ni-H2 state oxidised before the cleavage of H_2; b) Does an extra intermediate exist between the Ni-H2 and Ni-R states.[27, 28] Moreover, for the remaining part of the reaction, from Ni-C to Ni-SI_a, several additional reaction mechanisms (shown with blue arrows in Figure 2) have not been examined. In particular, it is not clear whether the Ni-L state is involved in the catalytic cycle or not.[18, 19] Moreover, it is unclear how the protein surroundings affect the reaction mechanism – several studies have suggested major effects of the surrounding protein and most recent QM-cluster studies employ large models (122–363).[20, 22, 27-32] In this paper, geometries were obtained with the QM/MM approach and the effect of the surroundings was estimated by big-QM calculations with 819 atoms in the QM system. QM/MM thermodynamic cycle perturbation (QTCP) calculations were carried out to obtain free energies between the various states. In addition, the DMRG-CASSCF approach was employed to investigate the electronic structure of some species.

Methods

The protein

The calculations were started from our previous QM/MM structure of the Ni-H2 state of [NiFe] hydrogenase, shown in Figure 1.[21] It was based on the 1.4-Å crystal structure from *D. vulgaris* Miyazaki F (PDB code 1H2R).[5] The protonation states of all residues were the same as in the previous structure and the fully protonated and solvated structure contained a total of 56 989 atoms.

QM calculations

DFT calculations were performed with the Turbomole 7.1 software.[33] The TPSS[34] and B3LYP[35-37] functionals were used, combined with the def2-SV(P),[38] def2-TZVP,[39] def2-TZVPD[40] and def2-QZVPD[39, 40] basis sets. The calculations were sped up by expanding the Coulomb interactions in an auxiliary basis set, the resolution-of-identity (RI) approximation.[41, 42] Empirical dispersion corrections were included with the DFT-D3 approach, standard zero-damping and optimised parameters for each DFT method,[43, 44] as implemented in Turbomole. The DFT calculations used a QM system consisting of the Ni and Fe ions with first-sphere ligands (CO, two CN^-, and four cysteine residues, modelled by CH_3S^-), as well as an acetic-acid model of Glu34 and an imidazole model of His88, as shown in Figure 1. Glu34 and His88 were included in the QM system because they form hydrogen bonds to the S ligands of the active-site metal ions and therefore tune their properties. Our previous studies have shown that they strongly influence the reaction energies.[45] Glu34 is also a putative proton acceptor of the active site. In most calculations, it was modelled in the

protonated form, donating a hydrogen bond to Cys546, because otherwise two negatively charged atoms are in close contact (cf. Figure 1).[45] However, when studying transfer of protons away from Cys546, Glu34 was deprotonated. All DFT calculations were performed with a point-charge model of the protein surroundings. All models were studied in their lowest spin state, viz. a singlet or doublet state, which according to our previous studies with multiconfigurational and coupled-cluster methods is the ground state of Ni-SI$_a$ and Ni-H2.[21, 22, 46] As can be seen in Table S2, we also checked the triplet or quartet states for the other intermediates and some transition states, and they were in general higher in energy, although in some cases, the two states are nearly degenerate. In future studies, we will study the spin-state ordering with more accurate methods.

DMRG-CASSCF calculations[47-50] were performed with the BLOCK code[48, 51-55] interfaced with MOLCAS 8.1.[56-58] They were performed to analyse the electronic structure of the I-B, Ni-R, Ni-C and I-D states. Thus, only single-point calculations in vacuum were performed. We used a small model for these calculations, obtained by replacing the four methyl groups on the Cys models by a proton, employing an S–H bond length of 1.34 Å, and removing the models of Glu34 and His88 in Figure 1, resulting in a QM region of 18 atoms. The calculations employed the ANO-RCC basis sets: [7s6p4d3f2g1h] for Ni and Fe,[59] [5s4p2d1f] for S,[60] [4s3p2d1f] for C, N, and O, and [3p1s] for H.[61] The number of renormalized states (m) was 1000 in all calculations. We used the default sweep schedule implemented in BLOCK, i.e. the initial DMRG iterations were done with a small m value to approximately converge the DMRG wavefunction, whereas the later iterations were carried out with the full m. A small amount of perturbative noise ($\varepsilon = 10^{-4}$) was added to the wavefunction in the initial iterations to prevent it from being trapped in a local minimum. The orbital ordering was automatized by minimising the quantum entanglement using a genetic algorithm.[62] Scalar relativistic effects were included using the second-order Douglas–Kroll–Hess Hamiltonian. An active space of 22 electrons in 22 orbitals was employed (details are given in the Results and Discussion section).

QM/MM calculations

The QM/MM calculations were performed with the ComQum software.[63, 64] In this approach, the protein and solvent are split into three subsystems: System 1 (the QM region) was relaxed by QM methods and it consisted of the same atoms as in the DFT calculations (Figure 1). System 2 consisted of all residues or water molecules within 6 Å of any atom in system 1. System 2 was optionally relaxed by a full MM minimisation in each step of the QM/MM geometry optimisation (otherwise it was keep fixed at the crystal coordinates). Finally, system 3 consisted of all the remaining parts of the protein and the solvent. It was kept fixed at the original (crystallographic) coordinates.

In the QM calculations, system 1 was represented by a wavefunction, whereas all other atoms were represented by an array of partial point charges, one for each atom, taken from MM libraries. Thereby, the polarization of the QM system by the surrounding protein is included in a self-consistent manner. When there is a bond between systems 1 and 2 (a junction), the hydrogen link-atom approach was employed: The QM system was capped with hydrogen atoms (hydrogen link atoms, HL), the positions of which are linearly related to the corresponding carbon atoms (carbon link atom, CL) in the full system.[63, 65] All atoms were included in the point-charge model, except the CL atoms.[31]

The total QM/MM energy in ComQum was calculated as[63, 64]

$$E_{\mathrm{QM/MM}} = E^{\mathrm{HL}}_{\mathrm{QM1+ptch23}} + E^{\mathrm{CL}}_{\mathrm{MM123},q_1=0} - E^{\mathrm{HL}}_{\mathrm{MM1},q_1=0} \quad (1)$$

where $E^{\mathrm{HL}}_{\mathrm{QM1+ptch23}}$ is the QM energy of the QM system truncated by HL atoms and embedded in a set of point charges modelling systems 2 and 3 (but excluding the self-energy of the point charges). $E^{\mathrm{HL}}_{\mathrm{MM1,q1=0}}$ is the MM energy of the QM system, still truncated by HL atoms, but without any electrostatic interactions. Finally, $E^{\mathrm{CL}}_{\mathrm{MM123,q1=0}}$ is the classical energy of all atoms in the system with CL atoms and with the charges of the QM system set to zero (to avoid double counting of the electrostatic interactions). Thus, ComQum employs a subtractive scheme with electrostatic embedding and van der Waals link-atom corrections.[66]

The geometry optimisation was continued until the energy change between two iterations was less than 2.6 J/mol (10^{-6} a.u.) and the maximum norm of the Cartesian gradients was below 10^{-3} a.u. The QM calculations were performed with Turbomole 7.1 software.[33] Geometry optimisations were performed with the TPSS[34] functional in combination with def2-SV(P)[38] basis set, including empirical dispersion corrections with the DFT-D3 approach.[67] The MM calculations were performed with Amber software,[68] using the Amber ff14SB force field.[69]

Big-QM calculations

Previous studies of [NiFe] hydrogenase have shown that both QM-cluster and QM/MM energies strongly depend on the size of QM system.[28, 31, 32] To avoid this problem, we have developed the big-QM approach:[29] We use a very big QM system consisting of all chemical groups with at least one atom within 4.5 Å of a minimal QM system (that shown in Figure 1, but without the Glu34 and His88 group) and junctions were moved at least two residues away from the minimal QM system. In addition, all charged groups buried inside the protein were included, but the three iron–sulfur clusters were omitted to avoid convergence problems, which according to our previous calculations can be done without compromising the energies.[29, 30] This gave a QM system of 819 atoms, shown in Figure 3.[22] All big-QM calculations were performed on coordinates from the QM/MM calculations and with a point-charge model of surroundings, because this gave the fastest calculations in our previous tests.[29] They also employed the multipole-accelerated resolution-of-identity J approach (marij keyword). The TPSS functional with the def2-SV(P) or def2-TZVP basis set were used in big-QM calculations.

To this big-QM energy, we added the DFT-D3 dispersion correction, calculated for the same big QM system with Becke–Johnson damping,[44] third-order terms and default parameters for the TPSS functional.[43, 44, 67] We also included a standard QM/MM correction for this large QM system (Eqn. 1, but with the big-QM region).

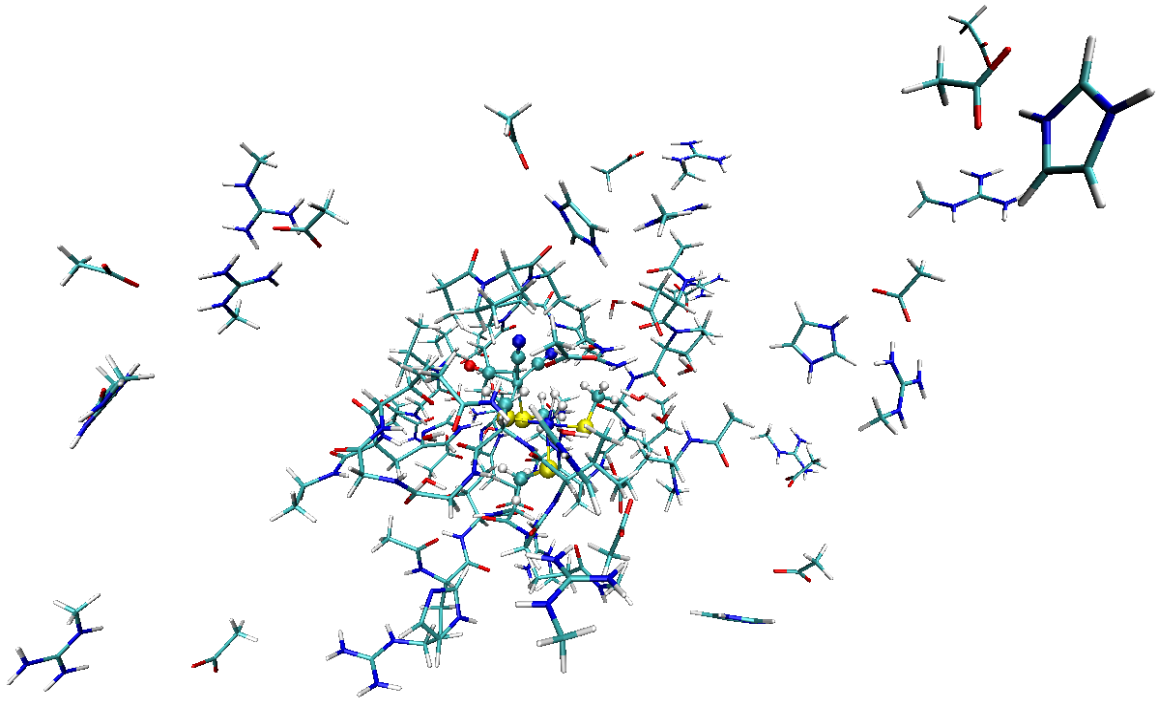

Figure 3. Atoms included in the big-QM calculations

QTCP calculations

The QTCP approach (QM/MM thermodynamic cycle perturbation) is a method to calculate free energy difference between two states, A and B, with a high-level QM/MM method, using sampling only at the MM level.[70-72] It employs the thermodynamic cycle in Figure 4, showing that the free-energy difference is obtained from three terms:

$$\Delta G_{\mathrm{QTCP}}(\mathrm{A} \rightarrow \mathrm{B}) = -\Delta G_{\mathrm{MM}\rightarrow\mathrm{QM/MM}}(\mathrm{A}) + \Delta G_{\mathrm{MM}}(\mathrm{A} \rightarrow \mathrm{B}) + \Delta G_{\mathrm{MM}\rightarrow\mathrm{QM/MM}}(\mathrm{B}) \qquad (2)$$

The QTCP calculations were performed as described before:[70, 71, 73] First, each state of interest was optimised with QM/MM, keeping system 2 fixed at the crystal structure. Then, the protein was further solvated in an octahedral box of TIP3P water molecules,[74] extending at least 9 Å from the QM/MM system. For one of the states, the system was first subjected to a 1000-step minimisation, keeping the atoms in the QM region fixed and restraining all heavy atoms in the crystal structure with a force constant of 418 kJ/mol/Å^2. Then, two 20-ps MD simulations were run with the heavy atoms still restrained. The first was run with a constant volume and the second with a constant pressure. Next, the size of the periodic box was equilibrated by a 100-ps MD simulation with a constant pressure and only the heavy atoms in QM region restrained to the QM/MM structure. Finally, for all states, an equilibration of 200 ps and a production simulation of 400 ps were run with a constant volume for each state. During the production run, snapshots were collected every 2 ps.

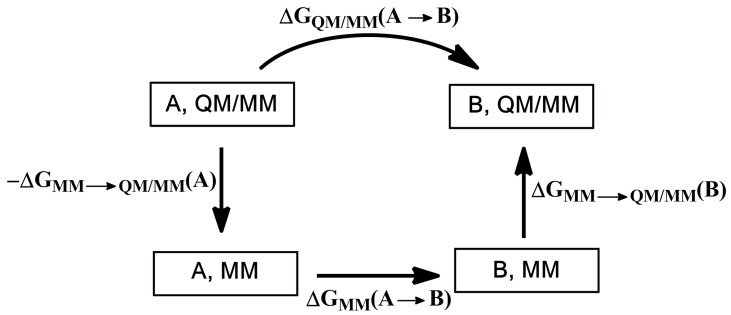

Figure 4. The thermodynamic cycle employed in the QTCP calculations

Based on these 200 snapshots, three sets of free-energy perturbations (FEPs) were performed, as shown in Figure 4. First, FEPs were performed at MM level in the forward and reverse directions along the reaction coordinate by changing the charges and coordinates of the QM region to those of the QM/MM calculations.[73] The charges were first modified in nine steps, keeping the coordinates at those of the A state. Then, the coordinates were modified in five steps to those of the B state (with the charges of the B state). Second, MM → QM/MM FEPs were performed for both the A and B states, keeping the QM regions fixed, as has been described before.[70, 71] All FEP calculations were performed with the local software calcqtcp. Further details of the QTCP calculations can be found in http://signe.teokem.lu.se/~ulf/Methods/qtcp.html.

Reported total energies are the big-QM energies, including dispersion and the MM contributions ($E_{\mathrm{bigQM/MM}}^{\mathrm{TPSS/SV(P)}}$ or $E_{\mathrm{bigQM/MM}}^{\mathrm{TPSS/TZVP}}$). This energy was extrapolated to the B3LYP method (which normally gives more accurate energies for both organic and bioinorganic systems) and the def2-QZVPD basis set using QM calculations of the standard QM system in Figure 1, including a point-charge model ($E_{\mathrm{QM}}^{\mathrm{B3LYP/SV(P)}} - E_{\mathrm{QM}}^{\mathrm{TPSS/SV(P)}}$ and $E_{\mathrm{QM}}^{\mathrm{TPSS/QZVPD}} - E_{\mathrm{QM}}^{\mathrm{TPSS/SV(P)}}$, where each energy term is $E_{\mathrm{QM1+ptch23}}^{\mathrm{HL}}$ in Eqn. 1, calculated with different DFT methods and basis sets, omitting the "def2-" prefix).[75, 76] Finally, the QTCP correction was added ($E_{\mathrm{QTCP}}^{\mathrm{TPSS/SV(P)}} - E_{\mathrm{QM/MM}}^{\mathrm{TPSS/SV(P)}}$), giving the final total energy:

$$E_{\mathrm{tot}} = E_{\mathrm{bigQM/MM}}^{\mathrm{TPSS/SV(P)}} + E_{\mathrm{QM}}^{\mathrm{TPSS/QZVPD}} + E_{\mathrm{QM}}^{\mathrm{B3LYP/SV(P)}} - 2E_{\mathrm{QM}}^{\mathrm{TPSS/SV(P)}} + E_{\mathrm{QTCP}}^{\mathrm{TPSS/SV(P)}} - E_{\mathrm{QM/MM}}^{\mathrm{TPSS/SV(P)}} \quad (3)$$

Results and Discussion

In this paper, we have studied the full reaction mechanism of [NiFe] hydrogenase by several QM methods, viz. the QM/MM, big-QM, QTCP and DMRG-CASSCF approaches. In the QM/MM calculations, the influence of the protein surroundings was taken into account by MM part. Big-QM calculations were employed to obtain converged and accurate energies based on the QM/MM-optimised geometries. All energies presented here are based on Eqn. 3 (big-QM energies, extrapolated to the B3LYP/def2-QZVPD basis set and including QTCP free-energy corrections) if not otherwise stated. In order to study the electronic structure of I-B, Ni-R, Ni-C and I-D, we used the DMRG-CASSCF method with a large active space. In this investigation, the Ni-H2 state was used as the starting state.

H_2 cleavage

As can be seen from Figure 2, cleavage of the H–H bond in Ni-H2 could give rise to the Ni-R state directly or go through the I-B state (the path via the I-A state was ignored because

previous studies indicated that the activation energy was 47 kJ/mol higher than for I-B).[27, 28] In the previous calculations, an energy barrier of 38 kJ/mol was obtained for the one-step reaction from QM-cluster calculations with 40 atoms, whereas for the rate-determining step of the two-step reaction, a barrier of 5 kJ/mol was obtained from QM-cluster calculations with 122 atoms.

With our QM/MM calculations, we could not find any direct reaction from Ni-H2 to Ni-R. Instead, cleavage of H_2 resulted in the I-B state, in agreement with the study by Bruschi and coworkers.[28] The energy barrier was 33 kJ/mol and the reaction was endothermic by 6 kJ/mol. The geometries were obtained from QM/MM optimisation with system 2 fixed. In I-B, the distances between the bridging hydrogen atom (H_b) and the two metals, Ni–H_b and Fe–H_b were 1.59 and 1.73 Å, respectively, and the distance between terminal hydrogen (H_t) and Ni ion, Ni–H_t, was 1.47 Å. We also tried calculations with system 2 relaxed and these gave nearly identical results with an energy barrier of 27 kJ/mol and a reaction energy of 10 kJ/mol. Our calculations indicate that the cleavage of H–H bond can take place with the Ni(II) ion, which is in agreement with the recent studies.[27, 28] In particular, the energy barrier of this step with Ni(II) ion is lower than in the previous studies with the Ni(III) or Ni(I) states, giving activation barriers of 36 and 49 kJ/mol, respectively.[25, 26]

In the I-B state, one of two hydrogen atoms bridges the two metals and this should be a hydride ion (H^-). However, the nature of the other hydrogen atom, which binds terminally to Ni with a Ni–H distance of 1.47 Å, is less clear: If it is also a hydride ion, the oxidation state of the Ni ion would be +IV, whereas if it is a proton, the Ni ion would remain in the +II state. In order to describe the electronic structure of the I-B state, we performed DMRG-CASSCF calculation with an active space of 22 electrons in 22 active orbitals, composed of two hydrogen 1s orbitals, three σ-bonding orbitals between the metal atoms and the coordinating ligand atoms, five Ni 3d, five Fe 3d and a second set of correlating 3d orbitals for each occupied metal orbital (which is often referred to as 3d') to account for the so-called double-shell effect (four on Ni and three on Fe), as shown in Figure 5.[77] It can be seen that three non-bonding 3d Ni orbitals are doubly occupied whereas both the fourth (mixed with the 1s orbital of the terminal hydrogen atom) and the fifth orbitals ($\sigma^*_{Ni\text{-}S}$) are empty. The orbital of the bridging hydride ion is mostly localised on the hydride ion and on the other ligands of the two metals, but with small contributions from the metals. Fe has three doubly occupied 3d orbitals, in accordance with an Fe(II) oxidation state. The natural populations on the two hydrogen atoms are similar. Therefore, the I-B species is best described as two hydride ions binding to a Ni(IV) ion, but with significant covalent character, especially for the terminal hydride ion.

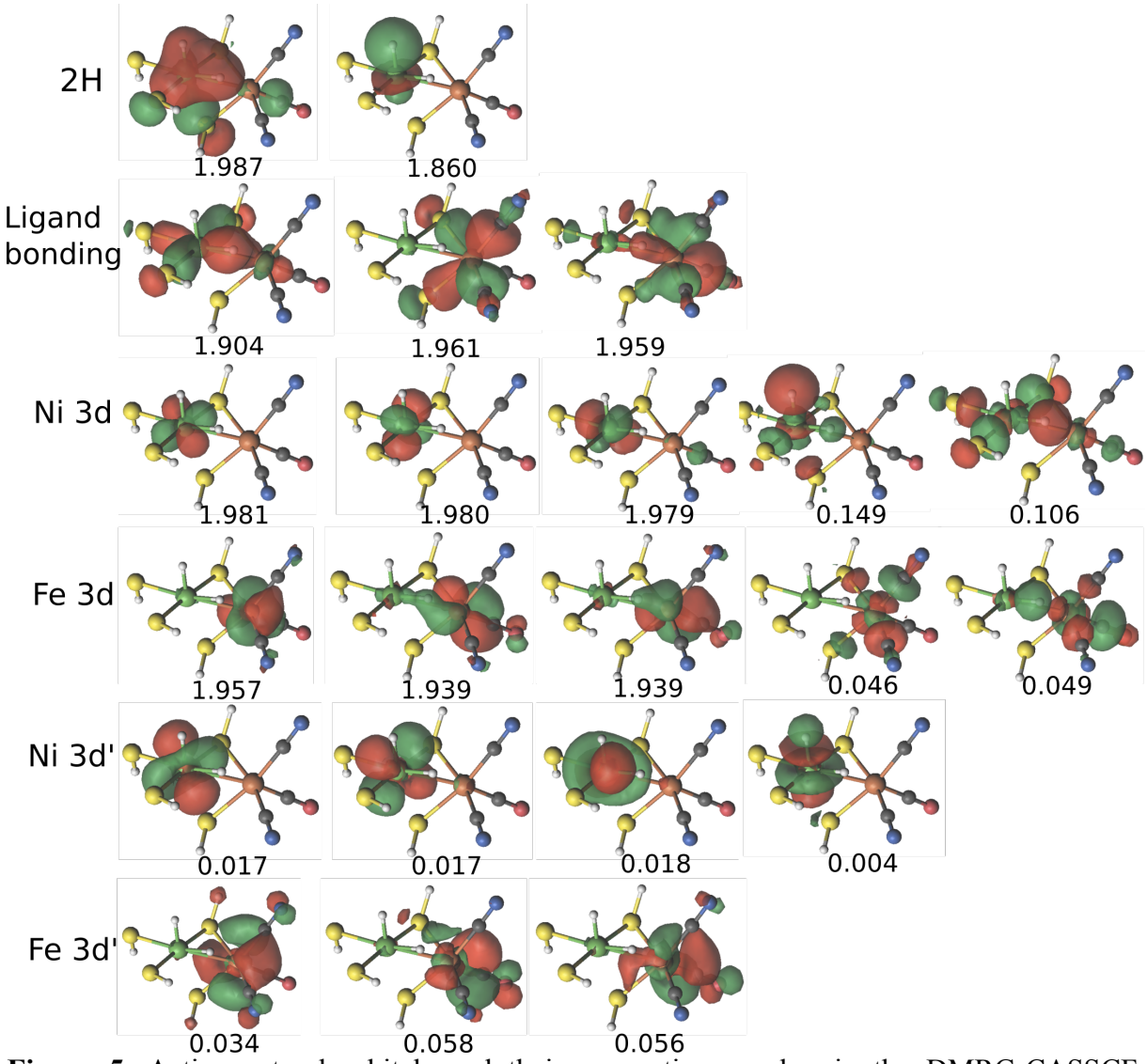

Figure 5. Active natural orbitals and their occupation number in the DMRG-CASSCF calculation of the I-B state.

Next, the terminal hydride ion was moved from Ni to the S atom of Cys546 to generate the Ni-R state with similar Ni–H_b and Fe–H_b distances as in the I-B state (1.60 and 1.71 Å). In Ni-R state, the oxidation state of Ni is back to +II (four of the 3d orbitals are doubly occupied) with a hydride bridging the two metals (Figure S1), indicating that the hydrogen moved to the Cys residue as proton coupled with the transfer of two electrons to Ni. The energy barrier is 18 kJ/mol and the reaction is exothermic by 44 kJ/mol. The full energy profile for the H_2-cleavage reaction is shown in Figure 6. Finally, the proton on Cys546 transfers to Glu34 (if the latter is deprotonated) without any barrier and a with a downhill QM/MM reaction energy of 101 kJ/mol, and it can then be transported out of the protein.

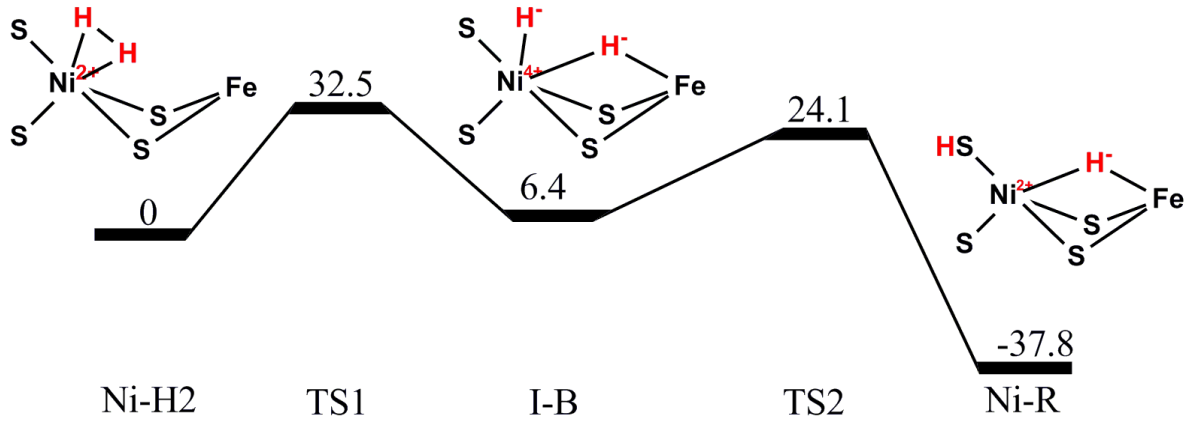

Figure 6. The reaction energy profile relative to the Ni-H2 state. Energies are E_{tot} (Eqn. 3) in kJ/mol obtained from QM/MM structures with system 2 fixed.

Reaction mechanism from Ni-C to Ni-SI$_a$

The Ni-C state is generated by a one-electron oxidation of the Ni-R state and dissociation of a proton (Figure 2). As is shown in Figure S2, three of Ni 3d orbitals are doubly occupied, one orbital is singly occupied and the fifth is empty. Thus, the oxidation state of Ni is +III and a hydride ion bridges the two metals. In the reaction of Ni-C→Ni-SI$_a$, it is unclear whether Ni-L is an intermediate state. In this work, we examined two possibilities.

First, we tried a reaction mechanism involving the Ni-L state. Following our previous study of the most favourable protonation state of Ni-L,[22] we assumed that the proton is on Cys546. For this mechanism, two pathways are conceivable (Figure 2), viz. a) that the hydride transfers directly to the S atom of Cys546, with a concomitant two-electron transfer to Ni, generating the Ni-L state with the Ni ion in the +I state or b) that the bridging hydride first moves to bind only to Ni, forming the I-C state, followed by its transfer from Ni to the S atom of Cys546.

In the previous study by Sun and coworkers using QM-cluster calculations with 180 atoms, the former mechanism was found to have an energy barrier of 64 kJ/mol and was endothermic by 29 kJ/mol.[27] However, in our QM/MM calculations, we could not locate any transition state or product (Ni-L). Instead, the energy increased monotonically as the H–S$_{546}$ distance was decreased, reaching 159 kJ/mol (relative to Ni-C state) at a distance of 1.3 Å. If the restraint was removed, the hydrogen atom moved back to bridge the two metals.

The energy profile of the latter mechanism, involving the I-C state, is shown in Figure 7. The total reaction is endothermic by 23 kJ/mol and the energy barrier is 89 kJ/mol. In the I-C state, the Ni–H bond length is 1.47 Å, i.e. the same as in the I-B state. The spin populations of 0.6, 0.2 and 0 on Ni, Fe and the hydrogen atom indicate that the hydrogen atom remains a hydride ion and the oxidation state of Ni is +III. An X-ray absorption study suggested that the oxidation state of Ni ion in Ni-L state is close to Ni(III).[17] Thus, the I-C species might be a candidate for this observed state. However, our results indicate that is unlikely that the Ni-L state can be formed from the Ni-C state, because the calculated activation barrier of 91 kJ/mol is too high when compared to the experimental net rate of the reaction, 750±90 s^{-1},[78] which corresponds to ~52 kJ/mol, according to transition-state theory (with a prefactor of 5.8·10^{12} s^{-1} and a temperature of 277 K).[79] Still, the results show that Ni-L is a local minimum on the potential-energy surface. Therefore, we tried the direct backward reaction from Ni-L to Ni-C. However, the results showed that also the backward reaction needs to go over the I-C intermediate state.

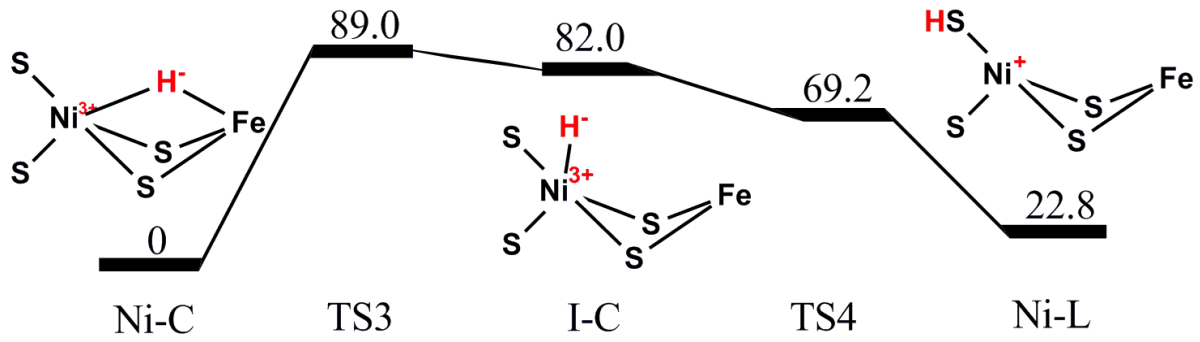

Figure 7. The reaction energy profile relative to the Ni-C state. Energies are E_{tot} (Eqn. 3) in kJ/mol.

Therefore, a reaction mechanism that does not involve the Ni-L state was also investigated. As shown in Figure 2, another electron and proton need to be removed from Ni-L to reach Ni-SI_a. Of course, it is then possible that the electron is first removed from the Ni-C state, before the hydride ion is converted to a proton on the Cys ligand. In the first intermediate of such a mechanism (after one-electron oxidation, called the I-D state), the Ni–H and Fe–H bond lengths are 1.63 and 1.67 Å, which are similar to those in the Ni-C state (1.62 and 1.69 Å). Interestingly, it can be seen from DMRG-CASSCF result (Figure S3) that one electron is transferred from the Fe ion to the Ni ion, indicating that the oxidation states of Ni and Fe ions in I-D are both +III. However, in our DFT calculations, this state, which corresponds to an open-shell singlet or a triplet state is 5–16 kJ/mol higher than the closed-shell (Ni^{4+}) state.

As shown in Figure 2, two possible mechanisms exist for the I-D→I-F reaction. Our QM/MM calculations indicate that cleavage of the Fe–H bond leads directly to I-F. In this reaction, the energy barrier is 58 kJ/mol relative to the I-D state and the I-F state is 31 kJ/mol more stable than I-D state. For the TS5 species, the Fe–H and H–S_{546} bond lengths are 2.6 and 1.9 Å. We also located the I-E state, but it is higher in energy than TS5 and therefore this indirect pathway is unfavourable. Finally, the proton is transferred from I-F to the deprotonated Glu34 without any energy barrier (if that residue is deprotonated), generating the Ni-SI_a state that is ready for the next cycle.

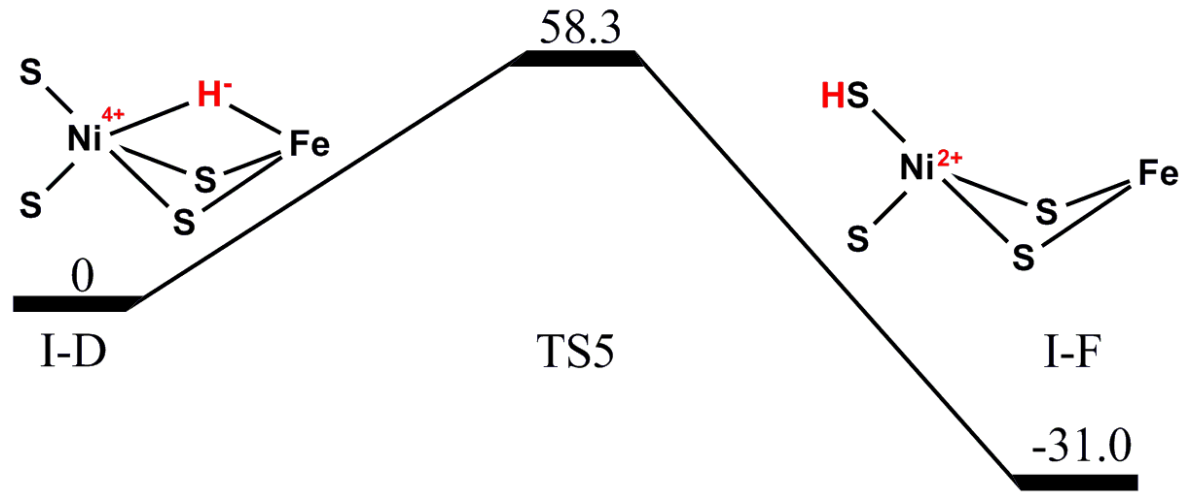

Figure 8. The reaction energy profile relative to the I-D state. Energies are E_{tot} (Eqn. 3) in kJ/mol.

Compared to the mechanism involving Ni-L (Figure 7), the I-D→I-F reaction gave lower reaction and activation energies, –31 and 58 kJ/mol, compared to +23 and 89 kJ/mol, respectively. Thus, according to our calculations, the most plausible reaction mechanism (shown in Figure 9) can be described as: 1) H_2 binds to the Ni(II) ion in the Ni-SI_a state; 2) the H–H bond is cleaved to generate the I-B state with a Ni(IV) ion and two hydride ions; 3) the hydride ion terminally bound to Ni moves to the S atom of Cys546 as a proton, coupled with a two-electron transfer to Ni, generating the Ni-R state with a Ni(II) ion; 4) one electron and one proton are removed from the system to form Ni-C state with a Ni(III) ion; 5) another electron is removed from Ni-C to generate the I-D state with a Ni(III) ion; 6) the bridging hydride ion transfers to the S atom of Cys546 as a proton and the two electrons transfer to Ni ion; 7) the second proton is removed from the system, resulting in the Ni-SI_a state to complete the catalytic cycle. Thus, the Ni-L state is not involved in this reaction mechanism. Based on our calculations, all hydrogen species bound to metal ions are best described as hydride ions, although the bonds involve a significant covalent character.

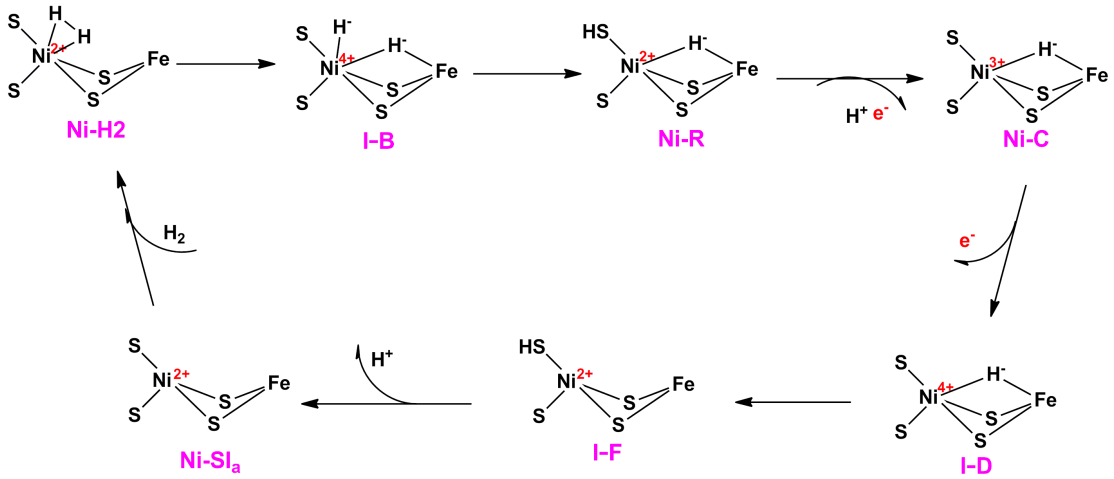

Figure 9. Reaction cycle of [NiFe] hydrogenase suggested by the present calculations.

Effects of the protein surroundings, basis set and DFT functional

According to previous studies, the reaction energies for [NiFe] hydrogenase are very sensitive to the size of the QM system.[21, 22, 27, 29-31] In this work, we compared energies from QM/MM, QM-cluster, big-QM and QTCP calculations (Table 1). It can be seen that the big-QM calculations change the energies by –2 to 11 kJ/mol, except for the I-F state, for which the correction is 60 kJ/mol. Thus, QM calculations with a large-size model are necessary to understand the reaction mechanism. The MM contribution of the big-QM energies is small (~1 kJ/mol) and the QTCP corrections are –12 to 2 kJ/mol.

The basis-set correction from def2-SV(P) to def2-QZVPD is –34 to 10 kJ/mol, indicating that the basis set has large effect on energy. We also tried to do QM calculations with the def2-TZVPD and def2-TZVP basis sets, and our results indicate that the energies are converged to within 2 kJ/mol at def2-TZVPD level and to within 3 kJ/mol with the def2-TZVP basis set.

The effect of the B3LYP method is varying. The largest effects were found for the I-B and I-F states, 24 and –78 kJ/mol respectively, whereas they are –15 to 7 kJ/mol for the other states. The large effect might be caused by the two-electron transfer from the hydride to Ni ion. In particular, for the reaction of I-D→I-F, the B3LYP method gives a high barrier for backward reaction. Thus, this process is very sensitive to the DFT methods.

Table 1. Relative energies (kJ/mol) obtained with the various methods (corresponding to the various terms in Eqn. 3). For clarity, the "def2-" prefix has been omitted for the basis sets.

	$E_{\mathrm{QM/MM}}$	E_{QTCP}	$E_{\mathrm{QM1}} = E^{\mathrm{HL}}_{\mathrm{QM1+ptch23}}$					$E_{\mathrm{Big\text{-}QM/MM}}$		E_{tot}
	TPSS SV(P)	TPSS SV(P)	TPSS SV(P)	B3LYP SV(P)	TPSS TZVP	TPSS TZVPD	TPSS QZVPD	TPSS SV(P)	MM	
Ni-H2	0	0	0	0	0	0	0	0	0	0
TS1	4.2	6.2	5.4	12.7	12.3	12.5	12.7	16.1	-0.2	32.5
I-B	-30.4	-36.5	-24.8	-0.8	-16.2	-15.7	-14.8	-20.5	-1.0	6.4
TS2	26.2	27.2	30.4	33.0	10.9	10.6	9.4	41.3	0.3	24.1
Ni-R	23.8	11.4	27.3	11.7	-3.9	-5.2	-6.4	25.4	-1.6	-37.8
I-D	0	0	0	0	0	0	0	0	0	0
TS5	74.8	74.3	72.9	58.6	66.1	65.9	65.5	81.4	-1.0	58.3
I-F	39.9	27.5	30.5	-47.7	1.2	0.4	-1.2	90.7	0.7	-31.0

Conclusions

In this paper, we have studied the full reaction mechanism of [NiFe] hydrogenase by means of a number of advanced computational methods, viz. QM/MM, big-QM, QTCP and DMRG-CASSCF. Geometries were optimised by QM/MM at the TPSS/def2-SV(P) level of theory. The effect of the protein surroundings was taken into account by big-QM calculations with 819 atoms in the QM system. Finally, the energies were extrapolated to the B3LYP/def2-QZVPD level by QM-cluster calculations with point-charge models and the QTCP corrections were added.

The calculations give many interesting clues for the reaction of [NiFe] hydrogenase. First, they indicate that the Ni-L state is not involved in the catalytic cycle of the hydrogen evolution reaction in [NiFe] hydrogenases. Instead, the Ni-C state needs to be oxidised by one electron to generate the I-D state because this state gives a lower reaction barrier for the transfer of the bridging hydride ion to Cys546 than the Ni-C state. In our calculations, this step is rate-determining with an energy barrier of 58 kJ/mol. In addition, the H–H cleavage involves an intermediate state I-B and the energy barrier is 33 kJ/mol for this process.

Second, our calculations suggest that metal-bound hydrogen species in all states in the reaction mechanism are best described as hydride ions, with a significant covalent character. The DMRG-CASSCF calculations indicated that oxidation states of the Ni ion in I-B, Ni-R and Ni-C states are +IV, +II, and +III, respectively.

Finally, our results showed that some of the reaction energies are sensitive to the size of the QM system for the [NiFe] hydrogenases. Therefore, it is currently not clear how transferable the present results are to [NiFe] hydrogenases from other organisms. Moreover, the basis-set effects (from def2-SV(P) to def2-QZVPD) were quite large (–32 to 9 kJ/mol), but the energies are converged to within 3 kJ/mol with the def2-TZVP basis set and the effect of diffuse functions in the basis set is small, ~2 kJ/mol. In addition, for the I-D→I-F reaction, the difference between the B3LYP and TPSS energies is very large, –78 kJ/mol. Thus, energies for reactions involving two-electron transfer to the metals may be very sensitive to the DFT methods. Consequently, high-level methods are required to obtain more accurate energies and such studies are currently performed in our group.

Supporting Information. Natural orbitals and occupation numbers for the Ni-R, Ni-C and I-D states. Energy components for the Ni-C → Ni-L reaction. Relative QM/MM energies of the high-spin states for all intermediates and TS5.

Acknowledgements

This investigation has been supported by grants from the Swedish research council (project 2014-5540), the Flemish Science Foundation (FWO, project G.0863.13), the China Scholarship Council and COST through Action CM1305 (ECOSTBio). QMP thanks funding from KU Leuven Postdoctoral mandates (PDM/16/112). The computations were performed on computer resources provided by the Swedish National Infrastructure for Computing (SNIC) at Lunarc at Lund University and by the VSC (Flemish Supercomputer Center), funded by the Hercules Foundation and the Flemish Government-department EWI.

References

(1) Lubitz, W.; Ogata, H.; Ruediger, O.; Reijerse, E. Hydrogenases. *Chem. Rev.* **2014,** *114*, 4081-4148.

(2) Bockris, J. O. M. The Hydrogen Economy: Its History. *Int. J. Hydrog. Energy* **2013,** *38*, 2579-2588.

(3) Yang, J. Y.; Bullock, M.; DuBois, M. R.; DuBois, D. L. Fast and Efficient Molecular Electrocatalysts for H_2 Production: Using Hydrogenase Enzymes as Guides. *MRS Bull.* **2011,** *36*, 39-47.

(4) Fontecilla-Camps, J. C.; Volbeda, A.; Cavazza, C.; Nicolet, Y. Structure/Function Relationships of NiFe- and FeFe-Hydrogenases. *Chem. Rev.* **2007,** *107*, 4273-4303.

(5) Higuchi, Y.; Ogata, H.; Miki, K.; Yasuoka, N.; Yagi, T. Removal of the Bridging Ligand Atom at the Ni–Fe Active Site of [NiFe] Hydrogenase Upon Reduction with H_2, as Revealed by X-Ray Structure Analysis at 1.4 Å Resolution. *Structure* **1999,** *7*, 549-556.

(6) Lubitz, W.; Reijerse, E.; van Gastel, M. NiFe and FeFe Hydrogenases Studied by Advanced Magnetic Resonance Techniques. *Chem. Rev.* **2007,** *107*, 4331-4365.

(7) Dole, F.; Fournel, A.; Magro, V.; Hatchikian, E. C.; Bertrand, P.; Guigliarelli, B. Nature and Electronic Structure of the Ni-X Dinuclear Center of Desulfovibrio Gigas Hydrogenase. Implications for the Enzymatic Mechanism. *Biochemistry* **1997,** *36*, 7847-7854.

(8) Huyett, J. E.; Carepo, M.; Pamplona, A.; Franco, R.; Moura, I.; Moura, J. J. G.; Hoffman, B. M. ^{57}Fe Q-Band Pulsed Endor of the Hetero-Dinuclear Site of Nickel Hydrogenase: Comparison of the NiA, NiB, and NiC States. *J. Am. Chem. Soc.* **1997,** *119*, 9291-9292.

(9) Foerster, S.; Stein, M.; Brecht, M.; Ogata, H.; Higuchi, Y.; Lubitz, W. Single Crystal EPR Studies of the Reduced Active Site of [NiFe] Hydrogenase from Desulfiovibrio Vulgaris Miyazaki F. *J. Am. Chem. Soc.* **2003,** *125*, 83-93.

(10) Ogata, H.; Nishikawa, K.; Lubitz, W. Hydrogens Detected by Subatomic Resolution Protein Crystallography in a [NiFe] Hydrogenase. *Nature* **2015,** *520*, 571-574.

(11) Pandelia, M.-E.; Ogata, H.; Lubitz, W. Intermediates in the Catalytic Cycle of NiFe Hydrogenase: Functional Spectroscopy of the Active Site. *ChemPhysChem* **2010,** *11*, 1127-1140.

(12) Fichtner, C.; van Gastel, M.; Lubitz, W. Wavelength Dependence of the Photo-Induced Conversion of the Ni-C to the Ni-L Redox State in the NiFe Hydrogenase of Desulfovibrio Vulgaris Miyazaki F. *Phys. Chem. Chem. Phys.* **2003,** *5*, 5507-5513.

(13) Medina, M.; Hatchikian, E. C.; Cammack, R. Studies of Light-Induced Nickel EPR Signals in Hydrogenase: Comparison of Enzymes with and without Selenium. *Biochim. Biophys. Acta-Bioenerg.* **1996,** *1275*, 227-236.
(14) Whitehead, J. P.; Gurbiel, R. J.; Bagyinka, C.; Hoffman, B. M.; Maroney, M. J. The Hydrogen Binding-Site in Hydrogenase: 35-Ghz ENDOR and XAS Studies of the Ni-C Active Form and the Ni-L Photoproduct. *J. Am. Chem. Soc.* **1993,** *115*, 5629-5635.
(15) van der Zwaan, J. W.; Albracht, S. P. J.; Fontijn, R. D.; Slater, E. C. Monovalent Nickel in Hydrogenase from Chromatium Vinosum: Light Sensitivity and Evidence for Direct Interaction with Hydrogen. *FEBS Lett.* **1985,** *179*, 271-277.
(16) Happe, R. P.; Roseboom, W.; Albracht, S. P. J. Pre-Steady-State Kinetics of the Reactions of [NiFe]-Hydrogenase from Chromatium Vinosum with H_2 and CO. *Eur. J. Biochem.* **1999,** *259*, 602–608.
(17) Davidson, G.; Choudhury, S. B.; Gu, Z. J.; Bose, K.; Roseboom, W.; Albracht, S. P. J.; Maroney, M. J. Structural Examination of the Nickel Site in Chromatium Vinosum Hydrogenase: Redox State Oscillations and Structural Changes Accompanying Reductive Activation and CO Binding. *Biochemistry* **2000,** *39*, 7468-7479.
(18) Hidalgo, R.; Ash, P. A.; Healy, A. J.; Vincent, K. A. Infrared Spectroscopy During Electrocatalytic Turnover Reveals the Ni-L Active Site State During H_2 Oxidation by a NiFe Hydrogenase. *Angew. Chem. Int. Ed.* **2015,** *54*, 7110-3.
(19) Murphy, B. J.; Hidalgo, R.; Roessler, M. M.; Evans, R. M.; Ash, P. A.; Myers, W. K.; Vincent, K. A.; Armstrong, F. A. Discovery of Dark pH-Dependent H^+ Migration in a [NiFe]-Hydrogenase and Its Mechanistic Relevance: Mobilizing the Hydrido Ligand of the Ni-C Intermediate. *J. Am. Chem. Soc.* **2015,** *137*, 8484-8489.
(20) Dong, G.; Ryde, U.; Jensen, H. J. A.; Hedegard, E. D. Exploration of H_2 Binding to the [NiFe]-Hydrogenase Active Site with Multiconfigurational Density Functional Theory. *Phys. Chem. Chem. Phys.* **2018,** *20*, 794-801.
(21) Dong, G.; Phung, Q. M.; Hallaert, S. D.; Pierloot, K.; Ryde, U. H_2 Binding to the Active Site of [NiFe] Hydrogenase Studied by Multiconfigurational and Coupled-Cluster Methods. *Phys. Chem. Chem. Phys.* **2017,** *19*, 10590-10601.
(22) Dong, G.; Ryde, U. Protonation States of Intermediates in the Reaction Mechanism of [NiFe] Hydrogenase Studied by Computational Methods. *J. Biol. Inorg. Chem.* **2016,** *21*, 383-394.
(23) Niu, S. Q.; Thomson, L. M.; Hall, M. B. Theoretical Characterization, of the Reaction Intermediates in a Model of the Nickel-Iron Hydrogenase of Desulfovibrio Gigas. *J. Am. Chem. Soc.* **1999,** *121*, 4000-4007.
(24) Pavlov, M.; Siegbahn, P. E. M.; Blomberg, M. R. A.; Crabtree, R. H. Mechanism of H−H Activation by Nickel−Iron Hydrogenase. *J. Am. Chem. Soc.* **1998,** *120*, 548-555.
(25) Pardo, A.; De Lacey, A. L.; Fernandez, V. M.; Fan, H. J.; Fan, Y. B.; Hall, M. B. Density Functional Study of the Catalytic Cycle of Nickel-Iron [NiFe] Hydrogenases and the Involvement of High-Spin Nickel(II). *J. Biol. Inorg. Chem.* **2006,** *11*, 286-306.
(26) Lill, S. O. N.; Siegbahn, P. E. M. An Autocatalytic Mechanism for NiFe-Hydrogenase: Reduction to Ni(I) Followed by Oxidative Addition. *Biochemistry* **2009,** *48*, 1056-1066.
(27) Qiu, S.; Azofra, L. M.; MacFarlane, D. R.; Sun, C. Hydrogen Bonding Effect between Active Site and Protein Environment on Catalysis Performance in H_2-Producing [NiFe] Hydrogenases. *Phys. Chem. Chem. Phys.* **2018,** *20*, 6735-6743.
(28) Bruschi, M.; Tiberti, M.; Guerra, A.; De Gioia, L. Disclosure of Key Stereoelectronic Factors for Efficient H_2 Binding and Cleavage in the Active Site of [NiFe]-Hydrogenases. *J. Am. Chem. Soc.* **2014,** *136*, 1803-1814.

(29) Hu, L.; Söderhjelm, P.; Ryde, U. Accurate Reaction Energies in Proteins Obtained by Combining QM/MM and Large QM Calculations. *J. Chem. Theory Comput.* **2013,** *9*, 640-649.
(30) Sumner, S.; Söderhjelm, P.; Ryde, U. Effect of Geometry Optimizations on QM-Cluster and QM/MM Studies of Reaction Energies in Proteins. *J. Chem. Theory Comput.* **2013,** *9*, 4205-4214.
(31) Hu, L.; Söederhjelm, P.; Ryde, U. On the Convergence of QM/MM Energies. *J. Chem. Theory Comput.* **2011,** *7*, 761-777.
(32) Hu, L.; Eliasson, J.; Heimdal, J.; Ryde, U. Do Quantum Mechanical Energies Calculated for Small Models of Protein-Active Sites Converge? *J. Phys. Chem. A* **2009,** *113*, 11793-11800.
(33) Turbomole V7.1 2016, a Development of University of Karlsruhe and Forschungszentrum Karlsruhe Gmbh, 1989-2007,
Turbomole Gmbh, since 2007; Available from http://www.turbomole.com.
(34) Tao, J.; Perdew, J. P.; Staroverov, V. N.; Scuseria, G. E. Climbing the Density Functional Ladder: Nonempirical Meta-Generalized Gradient Approximation Designed for Molecules and Solids. *Phys. Rev. Lett.* **2003,** *91*, 146401.
(35) Becke, A. D. Density-Fuctional Thermochemistry. III. The Role of Exact Exchange. *J. Chem. Phys.* **1993,** *98*, 5648-5652.
(36) Becke, A. D. Density-Functional Exchange-Energy Approximation with Correct Asymptotic-Behavior. *Phys. Rev. A* **1988,** *38*, 3098-3100.
(37) Lee, C. T.; Yang, W. T.; Parr, R. G. Development of the Colle-Salvetti Correlation-Energy Formula into a Functional of the Electron-Density. *Phys. Rev. B* **1988,** *37*, 785-789.
(38) Schäfer, A.; Horn, H.; Ahlrichs, R. Fully Optimized Contracted Gaussian-Basis Sets for Atoms Li to Kr. *J. Chem. Phys.* **1992,** *97*, 2571-2577.
(39) Weigend, F.; Ahlrichs, R. Balanced Basis Sets of Split Valence, Triple Zeta Valence and Quadruple Zeta Valence Quality for H to Rn: Design and Assessment of Accuracy. *Phys. Chem. Chem. Phys.* **2005,** *7*, 3297-3305.
(40) Rappoport, D.; Furche, F. Property-Optimized Gaussian Basis Sets for Molecular Response Calculations. *J. Chem. Phys.* **2010,** *133*, 134105.
(41) Eichkorn, K.; Treutler, O.; Öhm, H.; Häser, M.; Ahlrichs, R. Auxiliary Basis Sets to Approximate Coulomb Potentials. *Chem. Phys. Lett.* **1995,** *240*, 283-290.
(42) Eichkorn, K.; Weigend, F.; Treutler, O.; Ahlrichs, R. Auxiliary Basis Sets for Main Row Atoms and Transition Metals and Their Use to Approximate Coulomb Potentials. *Theor. Chem. Acc.* **1997,** *97*, 119-124.
(43) Grimme, S.; Antony, J.; Ehrlich, S.; Krieg, H. A Consistent and Accurate ab Initio Parametrization of Density Functional Dispersion Correction (DFT-D) for the 94 Elements H-Pu. *J. Chem. Phys.* **2010,** *132*, 154104.
(44) Grimme, S.; Ehrlich, S.; Goerigk, L. Effect of the Damping Function in Dispersion Corrected Density Functional Theory. *J. Comput. Chem.* **2011,** *32*, 1456-1465.
(45) Söderhjelm, P.; Ryde, U. Combined Computational and Crystallographic Study of the Oxidised States of NiFe Hydrogenase. *J. Mol. Struc. Theochem* **2006,** *770*, 199-219.
(46) Delcey, M. G.; Pierloot, K.; Phung, Q. M.; Vancoillie, S.; Lindh, R.; Ryde, U. Accurate Calculations of Geometries and Singlet-Triplet Energy Differences for Active-Site Models of NiFe Hydrogenase. *Phys. Chem. Chem. Phys.* **2014,** *16*, 7927-7938.
(47) White, S. R. Density-Matrix Formulation for Quantum Renormalization-Groups. *Phys. Rev. Lett.* **1992,** *69*, 2863-2866.

(48) Olivares-Amaya, R.; Hu, W. F.; Nakatani, N.; Sharma, S.; Yang, J.; Chan, G. K. L. The Ab-Initio Density Matrix Renormalization Group in Practice. *J. Chem. Phys.* **2015,** *142*, 034102.
(49) Wouters, S.; Van Neck, D. The Density Matrix Renormalization Group for Ab Initio Quantum Chemistry. *Eur. Phys. J. D* **2014,** *68*, 1-20.
(50) Marti, K. H.; Reiher, M. New Electron Correlation Theories for Transition Metal Chemistry. *Phys. Chem. Chem. Phys.* **2011,** *13*, 6750-6759.
(51) Chan, G. K. L.; Head-Gordon, M. Highly Correlated Calculations with a Polynomial Cost Algorithm: A Study of the Density Matrix Renormalization Group. *J. Chem. Phys.* **2002,** *116*, 4462-4476.
(52) Sharma, S.; Chan, G. K. L. Spin-Adapted Density Matrix Renormalization Group Algorithms for Quantum Chemistry. *J. Chem. Phys.* **2012,** *136*, 124121.
(53) Chan, G. K. L. An Algorithm for Large Scale Density Matrix Renormalization Group Calculations. *J. Chem. Phys.* **2004,** *120*, 3172-3178.
(54) Ghosh, D.; Hachmann, J.; Yanai, T.; Chan, G. K. L. Orbital Optimization in the Density Matrix Renormalization Group, with Applications to Polyenes and β-Carotene. *J. Chem. Phys.* **2008,** *128*, 014107.
(55) Zgid, D.; Nooijen, M. On the Spin and Symmetry Adaptation of the Density Matrix Renormalization Group Method. *J. Chem. Phys.* **2008,** *128*, 014107.
(56) Aquilante, F.; Autschbach, J.; Carlson, R. K.; Chibotaru, L. F.; Delcey, M. G.; De Vico, L.; Galvan, I. F.; Ferre, N.; Frutos, L. M.; Gagliardi, L.; Garavelli, M.; Giussani, A.; Hoyer, C. E.; Li Manni, G.; Lischka, H.; Ma, D. X.; Malmqvist, P. A.; Muller, T.; Nenov, A.; Olivucci, M.; Pedersen, T. B.; Peng, D. L.; Plasser, F.; Pritchard, B.; Reiher, M.; Rivalta, I.; Schapiro, I.; Segarra-Marti, J.; Stenrup, M.; Truhlar, D. G.; Ungur, L.; Valentini, A.; Vancoillie, S.; Veryazov, V.; Vysotskiy, V. P.; Weingart, O.; Zapata, F.; Lindh, R. Molcas 8: New Capabilities for Multiconfigurational Quantum Chemical Calculations across the Periodic Table. *J. Comput. Chem.* **2016,** *37*, 506-541.
(57) Phung, Q. M.; Wouters, S.; Pierloot, K. Cumulant Approximated Second-Order Perturbation Theory Based on the Density Matrix Renormalization Group for Transition Metal Complexes: A Benchmark Study. *J. Chem. Theory Comput.* **2016,** *12*, 4352-4361.
(58) Nakatani, N.; Guo, S. Density Matrix Renormalization Group (DMRG) Method as a Common Tool for Large Active-Space CASSCF/CASPT2 Calculations. *J. Chem. Phys.* **2017,** *146*.
(59) Roos, B. O.; Lindh, R.; Malmqvist, P.-Å.; Veryazov, V.; Widmark, P. O. New Relativistic Ano Basis Sets for Transition Metal Atoms. *J. Phys. Chem. A* **2005,** *109*, 6575-6579.
(60) Roos, B. O.; Lindh, R.; Malmqvist, P.-Å.; Veryazov, V.; Widmark, P. O. Main Group Atoms and Dimers Studied with a New Relativistic ANO Basis Set. *J. Phys. Chem. A* **2004,** *108*, 2851-2858.
(61) Widmark, P. O.; Malmqvist, P.-Å.; Roos, B. O. Density-Matrix Averaged Atomic Natural Orbital (ANO) Basis-Sets for Correlated Molecular Wave-Functions .I. 1st Row Atoms. *Theor. Chim. Acta* **1990,** *77*, 291-306.
(62) Moritz, G.; Hess, B. A.; Reiher, M. Convergence Behavior of the Density-Matrix Renormalization Group Algorithm for Optimized Orbital Orderings. *J. Chem. Phys.* **2005,** *122*.
(63) Ryde, U. The Coordination of the Catalytic Zinc Ion in Alcohol Dehydrogenase Studied by Combined Quantum-Chemical and Molecular Mechanics Calculations. *J. Comput. Aided Mol. Des.* **1996,** *10*, 153-164.

(64) Ryde, U.; Olsson, M. H. M. Structure, Strain, and Reorganization Energy of Blue Copper Models in the Protein. *Int. J. Quantum Chem.* **2001,** *81*, 335-347.
(65) Reuter, N.; Dejaegere, A.; Maigret, B.; Karplus, M. Frontier Bonds in QM/MM Methods: A Comparison of Different Approaches. *J. Phys. Chem. A* **2000,** *104*, 1720-1735.
(66) Cao, L.; Ryde, U. On the Difference between Additive and Subtractive QM/MM Calculations. *Front. Chem.* **2018,** *6*, 89.
(67) DFTD3 Software http://www.thch.uni-bonn.de/tc/index.php?section=downloads&subsection=dft-d3&lang=english.
(68) Case, D. A. Berryman, J. T. Betz, R. M. Cerutti, D. S. Cheatham, T. E. III, Darden, T. A. Duke, R. E. Giese, T. J. Gohlke, H. Goetz, A. W. Homeyer, N. Izadi, S. Janowski, P. Kaus, J. Kovalenko, A. Lee, T. S. LeGrand, S. Li, P. Luchko, T. Luo, R. Madej, B. Merz, K. M. Monard ,G. Needham, P. Nguyen, H. Nguyen, H. T. Omelyan, I. Onufriev, A. Roe, D. R. Roitberg, A. Salomon-Ferrer, R. Simmerling, C. L. Smith, W. Swails, J. Walker, R. C. Wang, J. Wolf, R. M. Wu, X. York, D. M. Kollman, P. A. (2014), AMBER 14, University of California, San Francisco.
(69) Maier, J. A.; Martinez, C.; Kasavajhala, K.; Wickstrom, L.; Hauser, K. E.; Simmerling, C. ff14SB: Improving the Accuracy of Protein Side Chain and Backbone Parameters from ff99SB. *J. Chem. Theory Comput.* **2015,** *11*, 3696-3713.
(70) Rod, T. H.; Ryde, U. Accurate QM/MM Free Energy Calculations of Enzyme Reactions: Methylation by Catechol O-Methyltransferase. *J. Chem. Theory Comput.* **2005,** *1*, 1240-1251.
(71) Rod, T. H.; Ryde, U. Quantum Mechanical Free Energy Barrier for an Enzymatic Reaction. *Phys. Rev. Lett.* **2005,** *94*, 138302.
(72) Luzhkov, V.; Warshel, A. Microscopic Models for Quantum-Mechanical Calculations of Chemical Processes in Solutions: LD/AMPAC and SCAAS/AMPAC Calculations of Solvation Energies. *J. Comput. Chem.* **1992,** *13*, 199-213.
(73) Heimdal, J.; Kaukonen, M.; Srnec, M.; Rulisek, L.; Ryde, U. Reduction Potentials and Acidity Constants of Mn Superoxide Dismutase Calculated by QM/MM Free-Energy Methods. *Chemphyschem* **2011,** *12*, 3337-3347.
(74) Jorgensen, W. L.; Chandrasekhar, J.; Madura, J. D.; Impey, R. W.; Klein, M. L. Comparison of Simple Potential Functions for Simulating Liquid Water. *J. Chem. Phys.* **1983,** *79*, 926-935.
(75) Blomberg, M. R. A.; Borowski, T.; Himo, F.; Liao, R.; Siegbahn, P. E. M. Quantum Chemical Studies of Mechanisms for Metalloenzymes. *Chem. Rev.* **2014,** *114*, 3601-3658.
(76) Curtiss, L. A.; Redfern, P. C.; Raghavachari, K. Assessment of Gaussian-3 and Density-Functional Theories on the G3/05 Test Set of Experimental Energies. *The J. Chem. Phys.* **2005,** *123*, 124107.
(77) Andersson, K.; Roos, B. O. Excitation-Energies in the Nickel Atom Studied with the Complete Active Space SCF Method and 2nd-Order Perturbation-Theory. *Chem. Phys. Lett.* **1992,** *191*, 507-514.
(78) Liebgott, P. P.; Leroux, F.; Burlat, B.; Dementin, S.; Baffert, C.; Lautier, T.; Fourmond, V.; Ceccaldi, P.; Cavazza, C.; Meynial-Salles, I.; Soucaille, P.; Fontecilla-Camps, J. C.; Guigliarelli, B.; Bertrand, P.; Rousset, M.; Leger, C. Relating Diffusion Along the Substrate Tunnel and Oxygen Sensitivity in Hydrogenase. *Nat. Chem. Biol.* **2010,** *6*, 63-70.
(79) Jesen, F. Introduction to Computational Chemistry. Wiley, Chichester, pp 454–464.

For Table of Contents Only

We have studied the reaction mechanism of [NiFe] hydrogenase with QM/MM, big-QM, QTCP and DMRG-CASSCF calculations. The results indicate that the Ni-L state is not involved in the mechanism. Instead the Ni-C state is reduced by one electron before the bridging hydride ion is transferred to Cys546 in a rate-determining step with a barrier of 58 kJ/mol. The energies are sensitive to the size of QM system, the basis set and the density-functional theory method.